Higher Vibrationally Excited Levels of the 3pπ $^2\Pi$ Rydberg State of HCO†

K. Prentice, R. Nicodemus, B. Rajaram, and E. R. Grant*

Department of Chemistry, Purdue University, West Lafayette, Indiana 47907

Received: June 4, 2004

Using the output of a frequency-tripled, pulsed dye laser, we have extended the ionization-detected one-photon absorption spectrum of HCO to include higher excited vibronic levels of the 3pπ $^2\Pi$ Rydberg state in the interval from 47 900 to 50 500 cm^{-1}. Included in this spectrum are band systems associated with bending overtones from (030) through (060), as well as cold-band transitions to bend−CO-stretch combinations from (011) through (031). The use of a separate, synchronized, fixed-frequency visible ionization pulse, in a technique that we term assisted REMPI, reveals a number of weak features. We find sequence-band transitions to confirmed states as well as to the higher excited levels, (041) and (070), which fall out of range as cold bands. We find a very weak structure that we assign to the (100)−(000) transition terminating on the CH-stretch fundamental. This band appears in the 3pπ state at a frequency very close to the value found for ω_1 in the HCO^+ cation. Continuing a trend established in earlier observations, we find that the Renner−Teller coupling of the electronic orbital and vibrational angular momentum in the 3pπ $^2\Pi$ state of HCO varies with bending quantum number, decreasing linearly with v_2 in both fundamental as well as bend−CO-stretch combination states.

I. Introduction

The effort to resolve structure and dynamics in molecular Rydberg states has benefited enormously from the simplification afforded by double-resonance spectroscopy.[1] In systems of Rydberg states near and above first ionization potentials, core-internuclear and single-electron orbital degrees of freedom approximately separate to support a very high density of states and rich coupling dynamics.[2] These dynamics figure centrally in important cation−electron transformations, such as autoionization and dissociative recombination.[3] Where available for such systems, spectroscopically assigned positions of resonant features provide a frequency-domain map of the coupling between electronic and rovibrational degrees of freedom. The acquisition of identifiable structure is important, and Franck−Condon diagonal photoselection serves well to isolate series built upon individual vibrational limits. For polyatomic systems in particular, photoselection has been essential to sort the relaxation dynamics associated with coupling in specific normal coordinates.[4]

Photoselecting individual vibrational−rotational levels in the intermediate 3pπ $^2\Pi$ Rydberg state, we have used double resonance to study high-Rydberg states converging to various vibrationally excited states of HCO^+.[5] We have been aided in this strategy by reference to the initial spectroscopic assignments of Cool and co-workers.[6,7] Building on this work, we have introduced a technique for this system that we term assisted REMPI,[8] in which a low-power UV laser is scanned to populate 3pπ states, while a subsequent pulse from a high-power fixed-frequency visible laser provides the energy to ionize this population. This process enhances the sensitivity with which we can detect rovibronic band systems. Our original assisted REMPI scans of 3pπ bands as high (030) reveal a number of weak transitions, which, when taken in combination with dominant structure, serve to refine spectroscopic parameters characterizing anharmonic and vibronic coupling, including a Renner parameter that varies with bending amplitude.[8]

These spectra reach wavelengths as short as 206 nm, the limit accessible by β-barium borate (BBO) frequency doubling. Our interest in the high-Rydberg states of HCO extends naturally to the spectroscopic characterization of autoionizing series built on higher vibrationally excited states of the core. To reach these higher vibrationally excited series, we must reach higher vibrationally excited gateway states at the 3pπ intermediate level. Ionization-detected two-photon absorption spectra recorded by Cool and co-workers establish the presence of resolvable structure as high as the tenth overtone of the bend.[6] Although revealing of certain higher band positions, two-photon absorption is not suitable as a means to prepare intermediate states for double resonance: A visible field at an intensity sufficient to drive two-photon absorption ionizes the intermediate population.

To form intermediate populations of states above (030) at sufficient density for double resonance requires one-photon excitation at wavelengths shorter than the BBO frequency-doubling limit. Such wavelengths can be produced in the range from 206 to 195 nm by frequency tripling. We have now added frequency tripling to the optical train for first-photon excitation and undertaken to perform scans over this higher energy interval. These scans resolve pure bending modes as high as the seventh overtone, together with a progression of combination bands where both the bending and CO-stretching modes are activated. With the improved signal-to-noise conferred by assisted REMPI, we also find weak structure that we can assign as the first evidence for the CH-stretching fundamental in this Rydberg gateway state.

II. Experiment

We record the high-resolution rovibrational spectrum of bands in the $X^2A'-3p\pi\ ^2\Pi$ system of HCO by means of (1+1′)-photon laser-assisted ionization-detected absorption spectroscopy (as-

† Part of the special issue "Tomas Baer Festschrift".

10.1021/jp040413c CCC: $27.50
Published on Web 10/20/2004

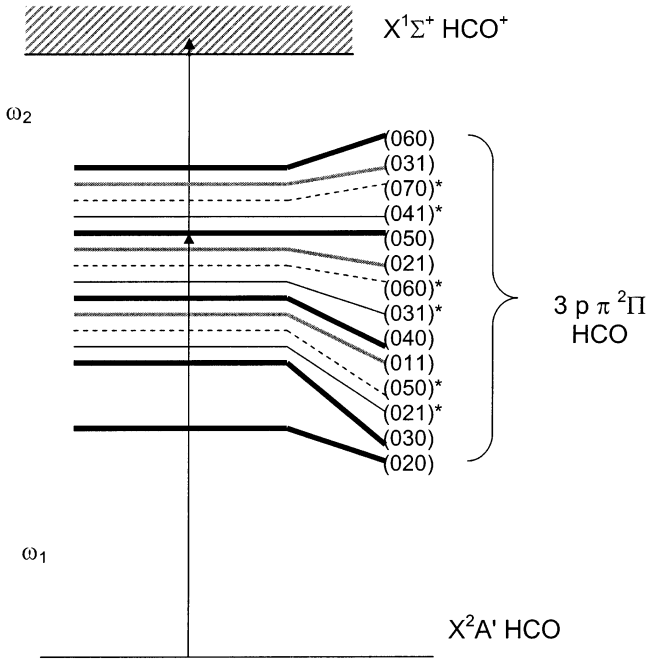

Figure 1. Energy level diagram illustrating the sequence of bands in the laser-assisted ionization-detected ultraviolet absorption spectrum in the 3pπ $^2\Pi \leftarrow X^2A'$ system of HCO. Levels labeled by asterisks appear as hot bands originating from the (010) vibrational level of the ground state.

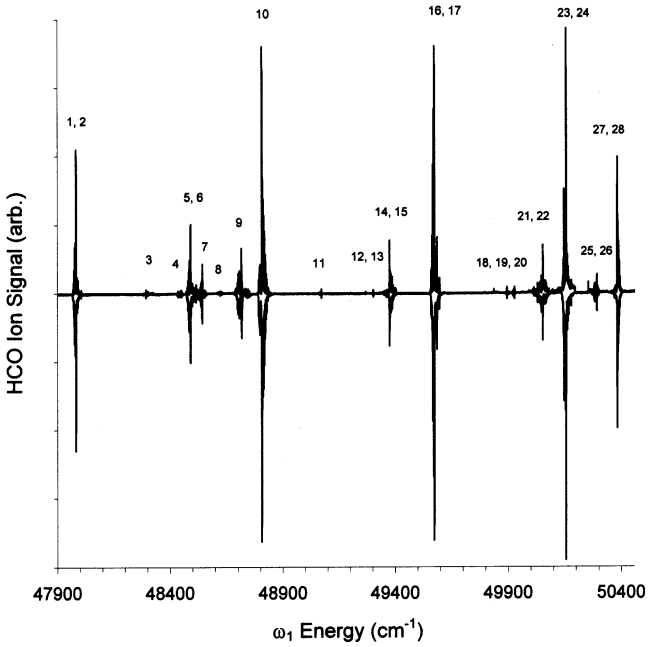

Figure 2. Composite view showing the ionization-detected, one-photon absorption spectrum of bands in the 3pπ $^2\Pi$ Rydberg state of HCO over the complete interval from 47 900 to 50 500 cm^{-1}. The top spectrum represents the experimental data, and the bottom spectrum is derived from simulation. Table 1 lists bands keyed to feature numbers.

sisted REMPI). Figure 1 shows an energy level diagram. Single rovibronic levels of the 3pπ $^2\Pi$ state, populated by ultraviolet first-photon absorption, are efficiently detected by high-power visible second-photon near-threshold photoionization.

Formyl radicals are produced by the photolysis of a precursor entrained in a pulsed free-jet expansion. A mixture of 15% acetaldehyde (CH_3CHO) vapor in N_2 is seeded at a stagnation pressure of 30 psig behind a solenoid valve (General Valve, IOTA-1). At the exit of the nozzle, a focused 308 nm pulsed XeCl excimer laser (Lambda Physik Compex 201) produces formyl radicals by photolysis. The expansion travels 8 cm to reach the ion collection region of a longitudinally mounted quadrupole mass spectrometer.

First-photon frequencies (ω_1) required to excite ground-state formyl radicals to successive bands of the 3pπ $^2\Pi$ Rydberg state are produced by frequency tripling the visible output of a 532 nm Nd:YAG-pumped dye laser (Continuum PL-7000 ND6000). The fundamental light is first frequency doubled by a Type I BBO (β-barium borate, β-BaB_2O_4) crystal housed in an INRAD Autotracker III. The second harmonic frequency component is rotated by 90° and combined with that of the fundamental to generate the sum frequency in a second BBO crystal housed in a separate INRAD Autotracker III.

Second-photon transitions ionize molecules excited to levels of the 3pπ $^2\Pi$ state by resonant first-photon absorption. Light for this step comes from a delayed counter propagating excimer-pumped dye laser (Lambda Physik EMG-201 MSC FL2002), operating at frequency of ω_2. ω_2 is set to a wavelength such that the total energy of ω_1 and ω_2 just exceeds the vertical ionization potential. Scanning ω_1 yields a spectrum of first-photon transitions. In this method of assisted resonant ionization spectroscopy, the high intensity of the visible laser, coupled with a large cross section for photoionization near threshold, improves the signal-to-noise ratio of the ionization-detected absorption spectrum.[9−11]

Ions produced by this excitation scheme are extracted and mass analyzed by a quadrupole mass spectrometer (Extrel Corp. Model 051-72). Mass-filtered HCO ions are detected by a channeltron particle multiplier (Galileo Type 4816), and the analog signal is conditioned by a current amplifier (Kiethley 427).

Calibration of the dye laser wavelengths occurs simultaneously as the experimental spectra are recorded. Laser excited neon lines are detected optogalvanically within an Fe/Ne hollow cathode lamp (Fischer Scientific). Neon transitions are compared to Ashworth and Brown's atlas of optogalvanic lines.[12] We determine photon energies from the vacuum corrected wavelengths with an absolute accuracy of ± 0.5 cm^{-1}.

III. Results

Figure 2 shows a composite view containing all of the ionization-detected, one-photon absorption spectra recorded in the present study of the 3pπ $^2\Pi$ Rydberg state of HCO. Earlier (1+1′)-REMPI scans of this system reach as high as 48 060 cm^{-1}.[8] Frequency tripling extends the range accessible to ionization-detected single-photon absorption to 50 505 cm^{-1}, allowing the observation of 26 new features. Table 1 shows a complete list of all the observed vibronic band origin energy positions in the 3pπ $^2\Pi \leftarrow X\ ^2A'$ transition system.

Note in Table 1 that transitions originating from $K'' = 0$ and $K'' = 1$ components of the X $^2A'$ (000) ground state redundantly determine energies for Σ^- and Σ^+ cold bands in the (010), (030), and (050) complexes. Table 1 also lists final-state absolute energies defined with reference to the X $^2A'$ ground state (000) level with $K'' = N'' = 0$ as a common origin.

Figure 2 evidences a bending progression that extends from (030) to (060). A bend−CO-stretch combination appears with members (011), (021), and (031). Several hot bands are also present originating from (010) in the HCO ground state, including distinctive transitions to (070) and (041). These hot bands serve to confirm the energy positions of the cold bands.

TABLE 1: Complete List of Transitions, Transition Energies, Simulated Transition Energies, and Absolute Energies for All Known Vibronic Band Origin Energy Positions in the $3p\pi\ ^2\Pi \leftarrow X^2A'$ System of HCO[a]

feature no.	transition	transition energy	simulated transition energy	absolute energy
(000)−(000)				
	$\Pi^+(1,0)$	45534.05	45533.7	45536.9
	$\Pi^+(1,1)$	45510.75	45511.07	45536.3
(010)−(000)				
	$\Sigma^-(0,1)$	46364.6	46365.5	46387.2
	$\Sigma^+(0,1)$	46247.8	46248.72	46270.4
	$\Sigma^-(0,0)$	46387.4	46388.1	46387.4
	$\Sigma^+(0,0)$	46270.85	46271.25	46270.8
	$\Delta^+(2,1)$	46302.4	46302.5	46333.5
	$\Delta^+(2,2)$	46234.8	46234.74	46334.1
(020)−(000)				
	$\Pi^-(1,0)$	47198.85	47198.7	47201.7
	$\Pi^+(1,0)$	47038.6	47038.5	47041.5
	$\Pi^-(1,1)$	47175.9	47175.8	47201.4
	$\Pi^+(1,1)$	47015.6	47015.9	47041.1
	$\Pi^-(1,2)$	47108.3	47108.2	47201.7
	$\Phi^+(3,2)$	47030.6	47030.63	47138.0
(030)−(000)				
1	$\Sigma^-(0,1)$	47983.4	47983.09	48005.5
	$\Sigma^+(0,1)$	47763.6	47763.6	47786.2
2	$\Sigma^-(0,0)$	48006.4	48005.7	48006.4
	$\Sigma^+(0,0)$	47785.95	47786.1	47786.0
	$\Sigma^-(0,2)$	47914.8		
	$\Delta^-(2,0)$	48007.5		48016.2
	$\Delta^-(2,1)$	47984.6	47984.4	48015.7
	$\Delta^+(2,1)$	47793.7	47791.8	47824.8
	$\Delta^-(2,2)$	47916.3	47916.7	48015.6
	$\Delta^+(2,2)$	47725.5	47724.03	47824.8
	$\Gamma^+(4,3)$	47718.6[b]	47718.6	47949.2
(040)−(000)				
10	$\Pi^-(1,0)$	48807.5	48807.7	48810.4
	$\Pi^+(1,0)$	48546.4[b]	48546.4	48549.3
	$\Pi^-(1,1)$	48784.9[b]	48784.9	48810.4
	$\Pi^+(1,1)$	48523.8[b]	48523.8	48549.3
9	$\Pi^-(1,2)$	48716.7	48717.45	48809.3
	$\Pi^-(1,3)$	48604		
(050)−(000)				
16	$\Sigma^-(0,1)$	49573.9	49573.54	49596.1
12	$\Sigma^+(0,1)$	49269	49268.7	49291.7
17	$\Sigma^-(0,0)$	49596.85	49596.02	49596.9
	$\Sigma^+(0,0)$	49291.3[b]	49291.3	49291.3
	$\Sigma^-(0,2)$	49505.6		
	$\Delta^-(2,0)$	49603.7		49612.4
	$\Delta^+(2,2)$	49227.1[b]	49227.13	49326.5
(060)−(000)				
28	$\Pi^-(1,0)$	50382.9	50382.9	50385.8
	$\Pi^+(1,0)$	50052.2[b]	50052.2	50055.1
27	$\Pi^-(1,1)$	50360.05	50360.05	50385.6
21	$\Pi^+(1,1)$	50029.8	50029.5	50055.7
26	$\Pi^-(1,2)$	50292.4	50292.7	50384.8
	$\Pi^-(1,3)$	50180.9		
(070)−(000)				
	$\Sigma^-(0,1)$	51135.4[b]	51135.4	51157.9
	$\Sigma^+(0,1)$	50765[b]	50765	50787.6
	$\Sigma^-(0,0)$	51157.9[b]	51157.9	51157.9
	$\Sigma^+(0,0)$	50787.55[b]	50787.55	50787.6
	$\Sigma^-(0,2)$	51068.8		
	$\Delta^-(2,0)$	51169.1		51177.8
(080)−(000)				
	$\Pi^-(1,1)$	51911.3		51936.8
	$\Pi^-(1,2)$	51844.5		51937.8
	$\Pi^-(1,3)$	51732		
(090)−(000)				
	$\Sigma^-(0,2)$	52607.6		
	$\Delta^-(2,0)$	52708.5		52717.2
(0100)−(000)				
	$\Pi^-(1,1)$	53437.1		53462.6
	$\Pi^-(1,2)$	53371.1		53464.4
	$\Pi^-(1,3)$	53258.5		
(001)−(000)				
	$\Pi^+(1,0)$	47708.9	47708.5	47711.8
	$\Pi^+(1,1)$	47685.55	47685.9	47711.1
(100)−(000)				
8	$\Pi^+(1,0)$	48622.3	48622.31	48625.2
(011)−(000)				
7	$\Sigma^-(0,1)$	48542.8	48542.8	48565.2
	$\Sigma^+(0,1)$	48419.3[b]	48419.3	48441.8
	$\Sigma^-(0,0)$	48565.4[b]	48565.4	48565.4
4	$\Sigma^+(0,0)$	48444.7[c]	48444.7	48444.7
	$\Delta^+(2,2)$	48408.5[b]	48408.5	48507.8
(021)−(000)				
15	$\Pi^-(1,0)$	49375.1	49375.1	49378.0
	$\Pi^+(1,0)$	49205.6[b]	49205.6	49208.5
14	$\Pi^-(1,1)$	49351.6	49352.4	49377.2
	$\Pi^+(1,1)$	49183	49182.98	49208.6
	$\Pi^-(1,2)$	49284.7[b]	49284.7	49378.1
	$\Pi^-(1,3)$	49180		
(031)−(000)				
23	$\Sigma^-(0,1)$	50155.8	50155.98	50178.2
20	$\Sigma^+(0,1)$	49927.7	49927.7	49949.9
24	$\Sigma^-(0,0)$	50178.8	50178.5	50178.8
	$\Sigma^+(0,0)$	49950.24[b]	49950.24	49950.2
	$\Sigma^-(0,2)$	50088.7		
(041)−(000)				
	$\Pi^-(1,0)$	50975.2[b]	50975.2	50978.1
	$\Pi^+(1,0)$	50705.8[b]	50705.8	50708.7
	$\Pi^-(1,1)$	50953.4	50952.62	50978.95
	$\Pi^+(1,1)$	50683.15[b]	50683.15	50708.7
	$\Pi^-(1,2)$	50885	50884.94	50978.35
	$\Pi^-(1,3)$	50773.5		
(051)−(000)				
	$\Sigma^-(0,2)$	51673.7		
	$\Delta^-(2,0)$	51771.8		51780.5
(061)−(000)				
	$\Pi^-(1,1)$	52524.8		52550.4
	$\Pi^-(1,2)$	52457.5		52550.8
	$\Pi^-(1,3)$	52345.4		
(071)−(000)				
	$\Sigma^-(0,2)$	53231		
	$\Delta^-(2,0)$	53329.9		53338.6
(010)−(010)				
	$\Sigma^-(0,1)$	45281.8	45282.4	46387.3
	$\Sigma^+(0,0)$	45189.8	45190.5	46270.6
(020)−(010)				
	$\Pi^-(1,0)$	46117.7[b]	46117.7	47201.3
(030)−(010)				
	$\Sigma^-(0,1)$	46899.97[b]	46899.97	48005.5
(040)−(010)				
	$\Pi^-(1,0)$	47726.7[b]	47726.7	48810.4
(050)−(010)				
5	$\Sigma^-(0,1)$	48490.95	48490.3	49596.2
6	$\Sigma^-(0,0)$	48515.75	48515.12	49596.5
(060)−(010)				
13	$\Pi^-(1,0)$	49302.6	49302.4	50386.2
(070)−(010)				
22	$\Sigma^-(0,1)$	50052.9	50052.2	51157.9
(011)−(010)				
	$\Sigma^-(0,1)$	47459.7[b]	47459.7	48565.2
(021)−(010)				
3	$\Pi^-(1,0)$	48293.84	48293.99	49377.5
(031)−(010)				
11	$\Sigma^-(0,1)$	49072.7	49072.7	50177.6
(041)−(010)				
19	$\Pi^-(1,0)$	49894.4	49894.6	50978.1
(020)−(020)				
	$\Pi^-(1,0)$	45058.4		
(030)−(020)				
	$\Sigma^-(0,1)$	45836.9		
(040)−(020)				
	$\Pi^-(1,0)$	46664.1		
(050)−(020)				
	$\Sigma^-(0,1)$	47426.5		
(020)−(001)				
	$\Pi^-(1,0)$	45330.4	45330.3	47201.4
(030)−(001)				
	$\Sigma^-(0,1)$	46114.6	46114.97	48005.2
(040)−(001)				
	$\Pi^-(1,0)$	46939.4[b]	46939.4	48810.4
(050)−(001)				
	$\Sigma^-(0,1)$	47705.4[b]	47705.44	49596.1
(040)−(011)				
	$\Pi^-(1,0)$	45860.3		
(050)−(011)				
	$\Sigma^-(0,1)$	46625.5		
18[d]		49837		
25[d]		50254.1		

[a] Absolute energies refer to $K'' = N'' = 0$ in the (000) ground state of HCO, and to K' in the upper state where $N' = K'$. Numbered features report transition energies measured in this work. Positions of other features are taken from the work of Cool et al.[6,7] or an average of the measured values from the work of Cool et al. and Robinson et al.[8] unless otherwise noted. [b] Calculated energies based on the spectroscopic constants of this work. Calculated energies are listed because either no experimental value is known or there is an uncertainty in either the assignment of the feature or the energy measurement. [c] The energy assignment listed is based on the R(0) peak of this $\Sigma^+(0,0)$ subband of (011). The band center is located at 48441.8 cm^{-1}. [d] Unidentified features; see text.

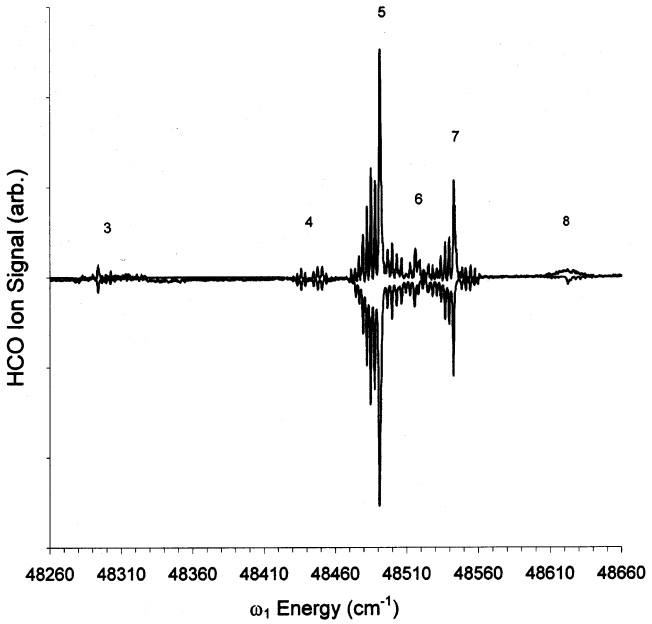

Figure 3. Ionization-detected, one-photon absorption spectrum of bands in the 3pπ $^2\Pi$ Rydberg state of HCO in the region of the Σ^- (0,1) (050)−(010) hot band (5) and the Σ^- (0,1) (011)−(000) combination band (7). The top spectrum represents the experimental data, and the bottom spectrum is derived from simulation. Feature numbers keyed to Table 1.

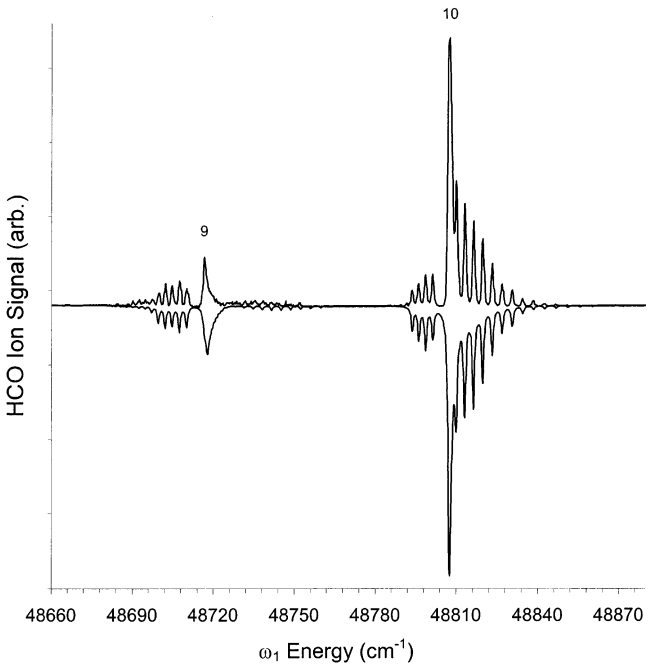

Figure 4. Ionization-detected, one-photon absorption spectrum of bands in the 3pπ $^2\Pi$ Rydberg state of HCO in the region of the Π^- (1,0) (040)−(000) cold band (10). The top spectrum represents the experimental data, and the bottom spectrum is derived from simulation.

Figures 3−7 show expanded views of selected regions. Band position 8 in Figure 3 marks the position of a weak feature that conforms exactly with the position predicted for the CH-stretch fundamental based on the frequency of this mode in the HCO ion.[13,14]

All but two of the discernible features in Figure 2 can be assigned, as indicated by negative-going simulations. These simulations build on a ground-state Hamiltonian established with exceeding accuracy by microwave and infrared spectroscopy. To derive an optimum set of upper-state spectroscopic constants,

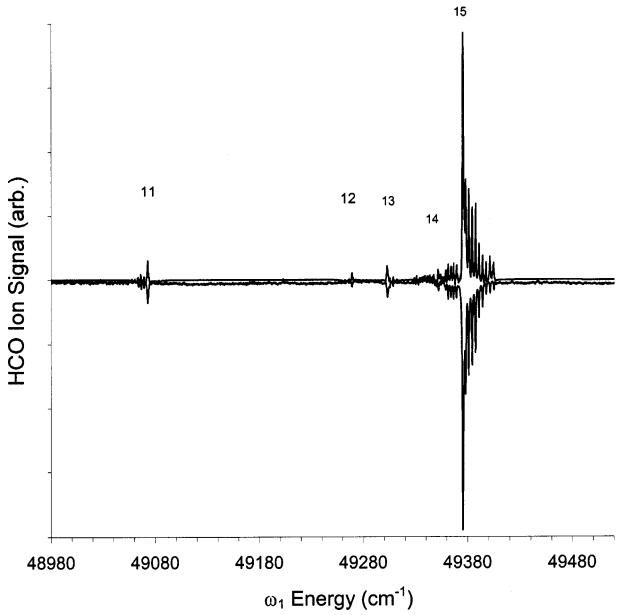

Figure 5. Ionization-detected, one-photon absorption spectrum of bands in the 3pπ $^2\Pi$ Rydberg state of HCO in the region of the Π^- (1,0) (021)−(000) combination band (15). The top spectrum represents the experimental data, and the bottom spectrum is derived from simulation.

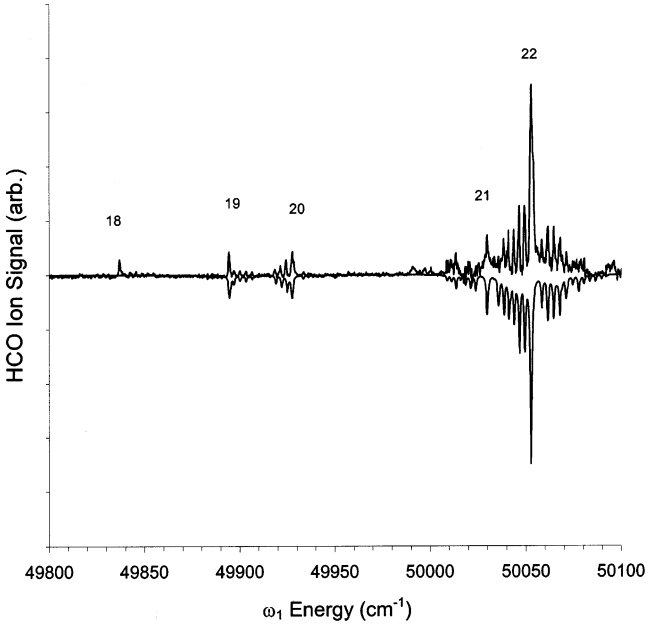

Figure 6. Ionization-detected, one-photon absorption spectrum of bands in the 3pπ $^2\Pi$ Rydberg state of HCO in the region of the Σ^- (0,1) (070)−(010) hot band (22). The top spectrum represents the experimental data, and the bottom spectrum is derived from simulation. Feature 18 cannot be assigned to any cold band or hot band originating from (010).

we adjust terms in the excited-state Hamiltonian for a linear triatomic molecule in a $^2\Pi$ state, starting from our earlier findings on the lower energy region of the (1+1′)-photon laser-assisted ionization-detected absorption spectrum as detailed below.[8]

IV. Discussion

A. Rotational Energy Levels of the X^{2}A′ (000) Ground State of HCO. The HCO radical has been extensively studied over the past 30 years by means of microwave and infrared spectroscopy. Brown and co-workers have compiled the results

TABLE 2: Spectroscopic Constants that Establish the Rotational Level Energies of the X²A′ (000), (010), and (001) States of HCO (in cm⁻¹)

		(000)	(010)	(001)
ν_o			1080.762	1868.1704
rigid rotor rotational constants				
	A	24.3296015	26.57498	24.228375
	B	1.4939571	1.500256	1.4814231
	C	1.3986631	1.392562	1.3871893
centrifugal distortion constants				
quartic centrifugal distortion	Δ_K	0.0314042	0.049561	0.031658
constant for $\Delta K = 0$	Δ_{NK}	1.5403×10^{-5}	-0.2×10^{-5}	1.594×10^{-5}
	Δ_N	3.9556×10^{-6}	3.22×10^{-6}	3.9299×10^{-6}
sextic centrifugal distortion	Φ_K	1.4677×10^{-4}	1.4677×10^{-4} [a]	1.516×10^{-4}
constant for $\Delta K = 0$	Φ_{KN}	-4.591×10^{-7}	-4.591×10^{-7} [a]	-5.08×10^{-7}
	Φ_{NK}	5.96×10^{-9}	5.96×10^{-9} [a]	5.96×10^{-9} [a]
principal axis election spin-rotation				
	ϵ_{aa}	0.3879660	0.47593	0.38816
	ϵ_{bb}	6.2379×10^{-4}	6.2379×10^{-4} [a]	5.99×10^{-4}
	ϵ_{cc}	-6.8674×10^{-3}	-6.8674×10^{-3} [a]	-6.908×10^{-3}
spin-rotation centrifugal distortion				
quartic terms for $\Delta K = 0$	Δ^s_K	-1.7308×10^{-3}	-3.160×10^{-3}	-1.657×10^{-2}
	$\Delta^s_{NK} + \Delta^s_{KN}$	-7.32×10^{6}	-7.32×10^{-6} [a]	-7.32×10^{-6} [a]
	Δ^s_N	1.040×10^{-7}	1.040×10^{-7} [a]	1.040×10^{-7} [a]
sextic terms for $\Delta K = 0$	Φ^s_K	1.158×10^{-5}	1.158×10^{-5} [a]	1.158×10^{-5} [a]

[a] Parameters fixed at the ground-state level.

from a number of observations to develop a refined set of rotational constants for the formyl radical ground state.[15] In addition, McKellar has listed the parameters for the first excited state in both the bending[16] and CO-stretch mode.[17] We draw on this base of information, as summarized in Table 2, to derive the constants used in our Hamiltonian for the X ^{2}A′ state.

The effective Hamiltonian for the X ^{2}A′ state of HCO can be constructed as a sum of asymmetric top contributions for rigid rotation, centrifugal distortion, spin-rotation, and spin-rotation centrifugal distortion. Expanding the effective Hamiltonian in a basis of prolate top wave functions yields matrix elements described by[18−21]

$$\langle NK|H_{\text{eff}}|NK\rangle = \left[A - \frac{1}{2}(B+C)\right]K^2 + \frac{1}{2}(B+C)N(N+1) - \Delta_K K^4 - \Delta_{NK}N(N+1)K^2 - \Delta_N N^2(N+1)^2 + \Phi_{NK}N^2(N+1)^2K^2 + \Phi_N N^3(N+1)^3 + \Phi_{KN}N(N+1)K^4 + \Phi_K K^6 - \frac{1}{2}[J(J+1) - N(N+1) - S(S+1)][a_o - a + 3aK^2/N(N+1)] + \left\{\frac{1}{2}[J(J+1) - N(N+1) - S(S+1)]/N(N+1)\right\}\{\Delta_K{}^S K^4 + (\Delta_{NK}{}^S + \Delta_{KN}{}^S)K^2N(N+1) + \Delta_N{}^S N^2(N+1)^2 + \Phi_K{}^S K^6\} \quad (1)$$

where $a_o = -(\epsilon_{aa} + \epsilon_{bb} + \epsilon_{cc})/3$ and $a = -(2\epsilon_{aa} - \epsilon_{bb} - \epsilon_{cc})/6$. For present purposes, we fix the sextic centrifugal distortion constant, Φ_N, to zero.[15] Off-diagonal elements of the Hamiltonian, which contribute negligibly for low values of J and K, are not included.

B. Rotational Structure of Vibrational Energy Levels in the 3pπ $^2\Pi$ Rydberg State of HCO. Renner−Teller splitting of vibrational levels lifts the electronic degeneracy in the 3pπ $^2\Pi$ state. As a consequence, the rovibronic Hamiltonian varies according to whether the upper-state total vibronic angular momentum, K, conforms to the condition, $K = 0$, $K = \upsilon_2 + 1$, or $0 \neq K \neq \upsilon_2 + 1$. In the 3p$\pi$ $^2\Pi$ state, K arises from the coupling between the orbital angular momentum of the Rydberg electron and the vibrational angular momentum of the linear

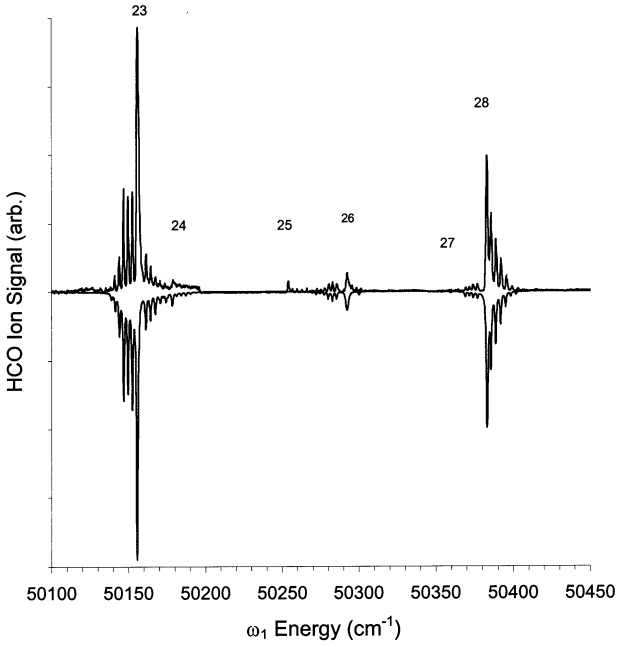

Figure 7. Ionization-detected, one-photon absorption spectrum of bands in the 3pπ $^2\Pi$ Rydberg state of HCO in the region of the Σ^- (0,1) (031)−(000) sequence band (23) and the Π^- (1,0) (060)−(000) cold band (28). The top spectrum represents the experimental data, and the bottom spectrum is derived from simulation. Feature 25 cannot be assigned to any cold band or hot band originating from (010).

cation core. This coupling gives rise to components with values

$$K = |\pm\Lambda \pm l| \quad (2)$$

where Λ and l represent molecular axis projections of the electronic orbital and vibrational angular momentum. For HCO in the 3pπ $^2\Pi$ electronic state, Λ has a value of 1. The range of l depends on the magnitude of the bending vibrational quantum number υ_2,

$$l = \upsilon_2, \upsilon_2 - 2, \upsilon_2 - 4, ..., -\upsilon_2 \quad (3)$$

As a result, for a Renner coupled Π electronic state, each bending excited vibrational level yields values of K defined by

$K = v_2 + 1$, $v_2 - 1$, $v_2 - 3$, ..., 1 or 0. $K = v_2 + 1$ determines a unique level and all other vibronic components form doublets split by Renner−Teller coupling. The vibronic energies of the unique level along a pure bending progression can be represented to second order by[22−24]

$$E(v_2,K,\Sigma) = [T_o - \omega - \chi_{22}] + \omega(v_2 + 1) + \chi_{22}(v_2 + 1)^2 + g_{22}K^2 + (g_k - 2g_{22})K + A\Sigma \quad (4)$$

where T_o is the difference in zero-point energies of the 3pπ $^2\Pi$ and ground states and χ_{22} is the anharmonic diagonal bending term. ω represents an effective bending frequency composed of the harmonic bending frequency and off-diagonal anharmonic bend−stretch terms:

$$\omega = \omega_2 + \frac{1}{2}\chi_{12} + \frac{1}{2}\chi_{23} \quad (5)$$

Because we have no way of measuring χ_{12} and χ_{23}, we adopt the convention of substituting ω as an effective fundamental frequency in expressions for excited-state vibronic energy. g_{22} is a quartic anharmonicity that splits vibrational angular momentum components and $A\Sigma$, with $\Sigma = \pm^1/_2$, represents the spin−orbit splitting. The term, g_k, defined by Brown,[25] arises from the K-dependent interaction of the various Renner vibronic components of the 3pπ state with levels of neighboring electronic states of Σ and Δ symmetry. The effect of this term is to alter the spacing between states of different K values in a given vibrational level. g_k typically has a value of a few cm^{-1}.

Nonunique levels with $K < v_2$ split to form pairs of bands with energies[22−24]

$$E(v_2,K,\Sigma) = [T_o - \omega - \chi_{22}] + \omega(v_2 + 1) + \chi_{22}(v_2 + 1)^2 + g_{22}K^2 \pm \sqrt{w^2 + [(g_k - 2g_{22})K + A\Sigma]^2} \quad (6)$$

where

$$w = \frac{\epsilon\omega}{2}\sqrt{(v_2 + 1)^2 - K^2} \quad (7)$$

in which ϵ is the Renner parameter appropriate to ω as an expression of the fundamental bending frequency.

1. Unique states with $K = v_2 + 1$. The total energy formula for a single vibrational subband, with $K = v_2 + 1$, is complete after adding a rotational energy expression to eq 4. Hougen has derived expressions for the rotational energy levels of a triatomic molecule in a $^2\Pi$ electronic state. To a first-order approximation, the energy levels for a unique subband are given by[26]

$$F\left(J{=}K{-}\frac{1}{2}\right) = C + BK - \frac{1}{2}A \quad (8)$$

$$F^{\pm}\left(J{>}K{-}\frac{1}{2}\right) = C + B\left[\left(J + \frac{1}{2}\right)^2 - K^2\right] \pm \frac{1}{2}\sqrt{4B^2\left(J + \frac{1}{2}\right)^2 + A_{eff}(A_{eff} - 4BK)} \quad (9)$$

with a second-order centrifugal distortion correction given by

$$E^{(2)} = -D\left(J + \frac{1}{2}\right)^4\left\{1 \pm 4\left[4\left(J + \frac{1}{2}\right)^2 + Y(Y - 4K)\right]^{-1/2}\right\} \quad (10)$$

where

$$A_{eff} = A\left[1 - \left(\frac{1}{8}\epsilon^2\right)K(K + 1)\right] \quad (11)$$

$$Y = \frac{A_{eff}}{B} \quad (12)$$

$$C = -(v_2 + 1)(v_2 + 2)\frac{\epsilon^2\omega}{8} \quad (13)$$

The state defined by $F(J{=}K{-}^1/_2)$ refers specifically to the lowest rotational level of the band system. This state is also designated as F_2 where $J = N - {}^1/_2$. The remaining F_2 spin components are given by the F^+ terms. The F^- terms define the positions of F_1 spin components for which $J = N + {}^1/_2$.

From our earlier work, the magnitude of the spin−orbit coupling constant, A, was found to be 1.8 cm^{-1}.[8] This value was derived from a fit of simulations to the unique state (010) $\Delta(2,1)$ for both HCO and DCO. The small magnitude of A indicates weak spin−orbit coupling which calls for a Hund's case (b) description for all vibronic levels.

2. Nonunique States with $K = 0$. For odd vibrational quanta, Renner−Teller coupling gives rise to a pair of $K = 0$ components of Σ^+ and Σ^- symmetry. The total energy levels for a subband with $K = 0$ is given by adding Hougen's derived expressions for a triatomic molecule in a $^2\Pi$ electronic state to eq 6. The rotational expressions for $K = 0$, in a rigid rotor limit for which the Renner−Teller splitting substantially exceeds the rotational spacing, are[26]

$$F_1(\kappa^2\Sigma,N) = C + \frac{1}{2}\gamma^\kappa + B_{eff}{}^\kappa N(N + 1) + \frac{1}{2}\gamma^\kappa N \quad (14)$$

$$F_2(\kappa^2\Sigma,N) = C + \frac{1}{2}\gamma^\kappa + B_{eff}{}^\kappa N(N + 1) - \frac{1}{2}\gamma^\kappa(N + 1) \quad (15)$$

$$F_1(\mu^2\Sigma,N) = C + \frac{1}{2}\gamma^\mu + B_{eff}{}^\mu N(N + 1) + \frac{1}{2}\gamma^\mu N \quad (16)$$

$$F_2(\mu^2\Sigma,N) = C + \frac{1}{2}\gamma^\mu + B_{eff}{}^\mu N(N + 1) - \frac{1}{2}\gamma^\mu(N + 1) \quad (17)$$

where F_1 and F_2 denote states for which $J = N + {}^1/_2$ and $N - {}^1/_2$, and the labels κ and μ refer to the Renner−Teller split Σ^+ and Σ^- vibronic components, respectively. Other terms are defined by

$$B_{eff}{}^\kappa = B[1 + (B/2r)\cos^2 2\beta] \quad (18)$$

$$B_{eff}{}^\mu = B[1 - (B/2r)\cos^2 2\beta] \quad (19)$$

$$\gamma^\kappa = 2B[1 - |\sin 2\beta| + (B/2r)\cos^2 2\beta] \quad (20)$$

$$\gamma^\mu = 2B[1 - |\sin 2\beta| - (B/2r)\cos^2 2\beta] \quad (21)$$

$$C = -(v_2 + 1)\frac{\epsilon^2\omega}{8} \quad (22)$$

in which

$$r\sin 2\beta = \frac{\epsilon\omega}{2}\sqrt{(v_2 + 1)^2 - K^2} \quad (23)$$

$$r\cos 2\beta = \frac{1}{2}A \quad (24)$$

and

$$r = \frac{1}{2}\sqrt{A^2 + [(v_2+1)^2 - K^2]\epsilon^2\omega^2} \tag{25}$$

Centrifugal distortion also affects the positions of higher rotational states. The following corresponding terms are added to the total rovibronic expression for a $K = 0$ subband,

$$E_1^{(2)}(\kappa^2\Sigma,N) = -\{D_{\text{eff}}{}^{\kappa}N^2(N+1)^2 + 2[D_{\text{eff}}{}^{\kappa} - D|\sin 2\beta|](N+1)^3] \tag{26}$$

$$E_2^{(2)}(\kappa^2\Sigma,N) = -\{D_{\text{eff}}{}^{\kappa}N^2(N+1)^2 - 2[D_{\text{eff}}{}^{\kappa} - D|\sin 2\beta|]N^3] \tag{27}$$

$$E_1^{(2)}(\mu^2\Sigma,N) = -\{D_{\text{eff}}{}^{\mu}N^2(N+1)^2 - 2[D_{\text{eff}}{}^{\mu} - D|\sin 2\beta|](N+1)^3] \tag{28}$$

$$E_2^{(2)}(\mu^2\Sigma,N) = -\{D_{\text{eff}}{}^{\mu}N^2(N+1)^2 + 2[D_{\text{eff}}{}^{\mu} - D|\sin 2\beta|]N^3] \tag{29}$$

where

$$D_{\text{eff}}{}^{\kappa} = D[1 + (2B/r)\cos^2 2\beta] \tag{30}$$

$$D_{\text{eff}}{}^{\mu} = D[1 - (2B/r)\cos^2 2\beta] \tag{31}$$

3. Nonunique States with $0 \neq K \neq v_2 + 1$. States for which the vibronic quantum number is neither zero nor $v_2 + 1$ form quartets, split by the interaction of vibrational and electronic angular momentum and by spin−orbit coupling. Hougen's derived rotational energy expressions for these states are added to eq 6 for the total energy formula. The principal bands split into identifiable Renner−Teller vibrational components, labeled κ and μ, with first-order rotational energies[26]

$$F\left(J{=}K{-}\frac{1}{2}\right) = C + BK \pm W \tag{32}$$

$$F\left(J{>}K{-}\frac{1}{2}\right) = C + B\left[\left(J+\frac{1}{2}\right)^2 - K^2\right] + \lambda_i \tag{33}$$

where

$$W = \frac{(v_2+1)KA\epsilon^2\omega}{16r}\cos^2 2\beta(B^2/2r) \tag{34}$$

and the eigenvalues λ_i are

$$\lambda(\kappa\pm) = \pm\sqrt{(W+BK)^2 + \sin^2 2\beta B^2\left[\left(J+\frac{1}{2}\right)^2 - K^2\right]} + \cos^2 2\beta(B^2/2r)\left[\left(J+\frac{1}{2}\right)^2 - K^2\right] \tag{35}$$

$$\lambda(\mu\pm) = \pm\sqrt{(W-BK)^2 + \sin^2 2\beta B^2\left[\left(J+\frac{1}{2}\right)^2 - K^2\right]} - \cos^2 2\beta\,(B^2/2r)\left[\left(J+\frac{1}{2}\right)^2 - K^2\right] \tag{36}$$

The $F(J{=}K{-}^1/_2)$ term given by eq 32 defines the first F_2 rotational line whereas substition of $\lambda(\kappa-)$ and $\lambda(\mu-)$ in eq 33 yields F_1 rotational energies. Values of $\lambda(\kappa+)$ and $\lambda(\mu+)$ determine the positions of the rest of the F_2 spin components.

C. Simulations of the Bands in the 3pπ $^2\Pi$ Electronic State of HCO. The expressions described above provide the basis for simulating the data shown in Figures 2−7 for the 3pπ $^2\Pi \leftarrow X^2A'$ transition in HCO. Simulated intensities are determined by means of assumed thermal population distributions over originating rotational levels, weighted by computed line strengths. Line strengths are assigned to all of the allowed transitions from each originating rotational state in accordance with Hönl-London factors[27] in the form extended by Kovaks[28] to include doublet−doublet spin multiplicity transitions. Lorentzians, weighted for population and line strength are then summed to make a simulated spectrum. The line widths are chosen to reflect the observed laser resolution.

Simulations use the value of T_o determined by Song and Cool[7] and confirmed in our assisted REMPI scans of the lower vibrational states.[8] χ_{22} is calculated, using eq 4, with the mean absolute energies of the Renner−Teller split pairs of Σ states associated with the (010), (030), and (050). Linear regression yields a value of -2.34 cm^{-1}. This anharmonicity yields a value of 797.5 cm^{-1} for the effective harmonic frequency, ω, as defined by eq 5.

We estimate g_k from the simulation by fitting transitions from ground state (000) $K'' = 1$ and 2 to the Δ component ($K' = 2$) of 3pπ (010). In the event that g_k were zero, the Renner formalism would predict a position of the Δ level for $v_2 = 1$ that falls below the mean energy of the split Σ pairs by an amount, $^1/_2\epsilon^2\omega$. However, according to Brown, if $4g_k > \epsilon^2\omega$, the energy of the Δ level can exceed the mean of the two Σ levels; the effect, in general, of a positive g_k, is to raise states of higher $|K|$ value relative to those of lower |K| with the same v_2.[25] Comparing the experimental absolute energies of the (010) Σ and Δ levels, we find that the energy of the Δ level indeed exceeds the average of the mean absolute energies of the two Σ Renner−Teller split pairs by about 5 cm^{-1}. Using experimentally derived values of χ_{22} and ω, we obtain a value of 1.41 cm^{-1} for g_k.

Analyzing the split positions in successive multiplets yields values for the Renner−Teller parameter, ϵ, and g_{22}. Robinson et al. reported the presence of a higher order contribution to the Renner−Teller coupling, represented by a vibrationally dependent Renner parameter that decreases with increasing vibrational amplitude.[8] Extending our observations to higher energy, we find that ϵ continues to decrease with v_2 according to the simple linear relationship,

$$\epsilon = 0.0764 - 0.0026v_2 \tag{37}$$

Figure 8 shows a plot of ϵ values determined from fits to simulations versus v_2. For (070), only one vibronic component in the split pair is observed. For this case, we estimate ϵ by choosing a position for the Σ^+ component that yields a $\Sigma^+ - \Sigma^-$ mean in conformance with our determination of χ_{22} and ω.

Equation 7, which gauges the magnitude of vibronic splitting as a function of ϵ, assumes a harmonic bending potential and a single-term expansion for the off-diagonal matrix element of the Renner Hamiltonian. Our measurements show that anharmonicity reduces the effective bending frequency as a function of v_2. This fits with the trend we see in the $\epsilon\omega$ product, which for constant ω defines a v_2-dependent ϵ. However, the relative magnitude of this apparent decrease is about 10 times greater than the proportional effect of anharmonicity on bending frequency, suggesting that higher order terms in the Renner Hamiltonian must play a significant role in reducing the apparent value of ϵ with increasing v_2.

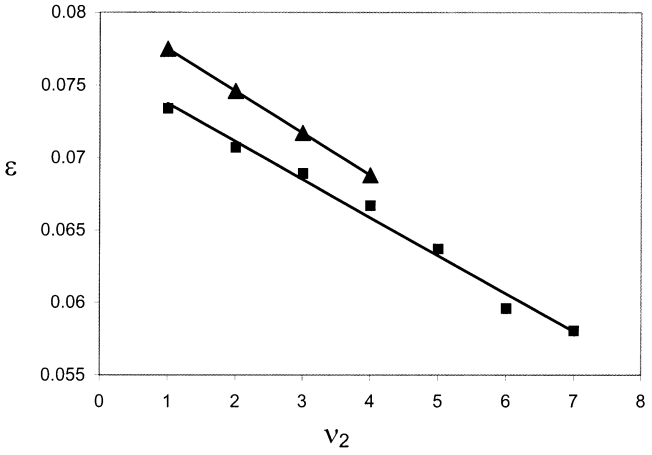

Figure 8. Plot illustrating the variation of the Renner parameter, ϵ, with υ_2 for vibronic complexes in the progression of pure bending states from (010) to (070) in the 3pπ $^2\Pi$ state of HCO (squares) and in the progression of bend−CO-stretch combination states from (011) through (041) (triangles).

For odd values of υ_2, the splitting between $K' = 0$ levels determines ϵ directly. For even values of υ_2, where no $K' = 0$ levels exist, ϵ cannot be measured independent of g_k- and g_{22}-dependent terms, which contribute to the splitting. Our analysis of the (010) $K' = 2$ unique level determines g_k independently from g_{22}. We assume a fixed value of this parameter for all simulations. Because we observe few high K subbands and the magnitude of g_k is only a few wavenumbers, residual υ_2 or K dependence would not discernibly alter Renner−Teller splittings at our resolution.

We allow g_{22} to vary with υ_2 and K. For example, we find that values of 4.6 and 6.1 cm^{-1}, respectively, best fit the Π and Φ Renner−Teller components of (020). According to Gauyacq and Jungen, g_{22} can be expected to exhibit a K-dependent contribution that increases with K much more rapidly than g_kK.[22]

For the (060) Π components, we provisionally assign a best-fit g_{22} value of 8.3 cm^{-1}. Though on balance, the parameter set we choose to characterize positions in this complex fits self-consistently with χ_{22} and trends in ϵ, the precise value of g_{22} is obscured by the uncertainty with which we are able to assign a precise origin for the $\Pi^+(1,1)$ subband.

Two hot band progressions appear in Figure 2 originating from (010) in the X ^{2}A′ ground state. One is a pure bending progression that extends from final state (050) to (070). The other is a combination progression that extends from (021) to (041). The assignment of these features is confirmed by agreement between experiment and simulated rotational structure represented by the appropriate expressions defined above.

The positions of excited-state combinations with CO stretch corresponded well with the energy of the 3pπ (001) CO-stretch fundamental (2174 cm^{-1}).[8] When one allows for the contribution of υ_2-dependent anharmonic cross terms, for example, we find that the added energy of the CO-stretch fundamental displaces the (041) complex of bands 2164 cm^{-1} to the blue of the corresponding structure observed for (040). We determine the Renner parameter for the (041) band from the linear regression of ϵ versus υ_2 for the set of bending combinations with $\upsilon_3 = 1$, which fits with

$$\epsilon = 0.0804 - 0.0029\upsilon_2 \qquad (38)$$

We assign the weak feature at 3088.26 cm^{-1} to the (100) CH-stretch fundamental based on the energy of this mode in the HCO ion (3088.74 cm^{-1}).[13,14] The ionization-detected absorption spectrum of this feature shows little rotational structure by which to confirm this assignment. The question arises as to why scans over this region do not produce a more distinctive signature of this vibrationally excited state. Weak signal could perhaps reflect 3pπ intermediate state dissociation, or an unfavorable Franck−Condon factor for the (100)−(000) transition. We have no way of monitoring dissociative loss, but we can estimate approximate Franck−Condon factors. Modeling the CH stretch of HCO as a diatomic local mode, we calculate approximate Franck−Condon factors using Henderson's recursion relations.[29] For the 3pπ $^2\Pi$ state we assume the 1.0935 Å equilibrium C−H bond length of the ion and a vibrational frequency of 3222.52 cm^{-1}.[30] For the X^{2}A′ ground state we use the known values of 1.119 Å and 2790 cm^{-1}.[31,32] These similarities in C−H bond length and vibrational frequency ensure vertical transitions in this mode, and our simple model returns a Franck−Condon factor for the (100)−(000) transition that is 0.026 times that of the origin band.

For comparison, we have computed the Franck−Condon factor for a transition to the 3pπ level excited by one quantum of CO stretch. Our quasi-diatomic approach yields a relative Franck−Condon factor of 0.9, which can be compared with a value of 1.05 determined from integrals over variational wave functions carried out by Peyerimhoff and co-workers.[33]

A simulation employing the self-consistent set of spectroscopic parameters presented here fits the entire spectrum of assigned rovibronic transitions with an average deviation of less than 1 cm^{-1}. Only two very weak features remain unassigned. Features 18 and 25 (at 49 837 and 50 254 cm^{-1}, respectively) fail to conform with any allowed transition originating from the zero-point level of ground-state HCO X ^{2}A′. Feature 18 falls within 30 cm^{-1} of the position that can be predicted for the (051) Σ^-−(001) sequence band. Feature 25 fits approximately with the calculated energy of the (032) Σ^+−(001) sequence band. Even allowing for uncertainty in associated off-diagonal anharmonicities, these matches are not convincing, particularly because they are unsupported by companion structure at other levels of the bend. The singular nature of these weak features also argues against assignment to an interloping electronic state. For the present purposes we regard them as probable artifacts and exclude them from the assignment.

A refined set of spectroscopic constants for pure bending in the 3pπ $^2\Pi$ state, based on the present work, is offered in Table 3. Rotational constants, shown to vary according to the value of K in relation to υ_2, are summarized in Table 4. In general terms, we find the Π subbands of all even vibronic levels described by a rotational constant within the range of 1.49 ± 0.021 cm^{-1}. The Σ features of odd subbands conform with a B ranging over the interval 1.475 ± 0.021 cm^{-1}. Higher K, Δ, Φ, and Γ subbands fit with a B value of 1.51 ± 0.0094 cm^{-1}. That the K dependence of B is stronger than the υ_2 dependence indicates a negligible bending vibration−rotation interaction

TABLE 3: Spectroscopic Constants for the 3pπ $^2\Pi$ State of HCO Compared with Previous Work (in cm^{-1})

	Song and Cool	Robinson et al.	present work
w	799.9	795.3	797.5
ν_3	2175	2174.3	
ν_1			3088.26
T_o	45540.1	45540.1	45540.1[a]
χ_{22}	−3.3	−1.88	−2.34
g_{22}	4.95	5.6	6.1[b]
g_k	−2.11	1.93	1.41
A	0.9	1.8	1.8[a]

[a] The values for T_o and A used in the simulation of the data were not determined from the present work. [b] An average value for g_{22}.

TABLE 4: Rotational Constants for the HCO 3pπ $^2\Pi$ State Determined by Comparison with Simulations of the 3pπ $^2\Pi \leftarrow X^2A'$ Transition (in cm^{-1})

		$K = 0$ (cm^{-1})	$0 \neq K \neq \upsilon_2 + 1$ (cm^{-1})	$K = \upsilon_2 + 1$ (cm^{-1})
(000)[a]	Π			1.485
(010)[a]	Σ^+	1.479		
	Σ^-	1.448		
	Δ			1.505
(020)[a]	Π		1.492	
	Φ			1.510
(030)[a]	Σ^+	1.495		
	Σ^-	1.464		
	Δ		1.527	
	Γ			1.515
(001)[a]	Π			1.530
(040)	Π		1.493	
(050)	Σ^-	1.497		
(060)	Π		1.48	
(011)	Σ^+	1.46		
	Σ^-	1.45		
(021)	Π		1.492	
(031)	Σ^-	1.46		

[a] Rotational constants for (000) through (030) and (001) determined by Robinson et al.

constant at our resolution. Such a dependence of B on Renner−Teller K has been seen in NCO by Kawaguchi et al.[34] and explained very recently by Brown.[35]

Transition energies determined by calculations using the spectroscopic constants refined in this work are compared with experimental observations in Table 1. The value measured in the present work for the energy of the (040), $\Pi^-(1,2)$ transition is deemed more accurate than the band position estimated from the (2+1)-photon ionization spectrum by Cool and co-workers.[6] For reference, Table 1 includes calculated energies based on the present experimentally calibrated Hamitonian for other band positions either unobserved or indistinctly observed in our scans, including the cold bands $\Pi^+(1,0)$ (040), $\Pi^-(1,1)$ (040), $\Delta^+(2,2)$ (011), and $\Pi^-(1,2)$ (021), as well as the $\Sigma^-(0,1)$ (050) and $\Pi^-(1,0)$ (040) hot bands originating from (001) in the ground state. Computed positions are also given for various hot bands originating from the (010) excited bending level of the ground state, including transitions to $\Pi^-(1,0)$ (020), $\Sigma^-(0,1)$ (030), $\Pi^-(1,0)$ (040), and $\Sigma^-(0,1)$ (011). For these cases, we believe that the calculated energies should be considered more accurate than experimentally derived estimates owing to unresolved rotational structure in the (1+1)- and (2+1)-photon ionization spectra.[6,7]

Similarly, we include calculated values for the energies of the cold subbands $\Gamma^+(4,3)$ in (030) and $\Delta^+(2,2)$ in (050). For $\Gamma^+(4,3)$ (030) in particular, simulations suggest a position more than 100 cm^{-1} below the energy assigned to this feature in the work by Robinson et al.[8] For $\Delta^+(2,2)$ (050), the calculated value differs by 27 cm^{-1} from the experimental position assigned in the (2+1)-photon work.[6]

The values we obtain for ω and χ_{22} fall between those reported by Song and Cool and Robinson et al. Song and Cool incorporated their (2+1)-photon ionization detected absorption data along with their (1+1)-photon results to extend their nonlinear least-squares fit of the bending progression in the 3pπ $^2\Pi$ state from (000) to (0100). They derive a value for χ_{22} that is slightly more negative than ours, whereas the value determined by Robinson et al. is more positive. The value for ω calculated in the present work is slightly smaller than the value determined by Song and Cool and larger than the value obtained by Robinson et al. The constants obtained by Robinson et al. were based on assisted REMPI band positions extending from (000) to (030) in the 3pπ $^2\Pi$ state. The present work extends the scope of this assignment to include bands from (040) to (070) in the upper state. As more vibronic levels are considered in fitting the data, we find a more negative χ_{22} and a larger ω. One can anticipate that a further extension of our data set will yield values for ω and χ_{22} that could well converge with those of Song and Cool.

Acknowledgment. This paper is based on work supported by the National Science Foundation under Grant No. CHE-0075833.

References and Notes

(1) Ebata, T.; Mikami, N.; Ito, M. *J. Chem. Phys*. **1983**, *78*, 1132. Cheung, W. Y.; Chupka, W. A.; Colson, S. D.; Gauyacq, D.; Avouris, P.; Wynne, J. J. *J. Chem. Phys*. **1983**, *78*, 3625. Gittins, C. M.; Harris, N. A.; Hui, M.; Field, R. W. *Can. J. Phys./Rev. Can. Phys*. **2001**, *79*, 247.

(2) Child, M. S.; Ed. *Molecular Rydberg Dynamics*; Imperial College Press: London, 1999. Sandorfy, C., Ed. *The Role of Rydberg States in Spectroscopy and Photochemistry*; Kluwer Academic: Dordrecht, The Netherlands, 1999.

(3) Ng, C. Y. *Annu. Rev. Phys. Chem*. **2002**, *53*, 101. Guberman, S. L., Ed.; *Dissociative Recombination of Molecular Ions with Electrons*; Kluwer Academic: Dordrecht, The Netherlands, 2003

(4) Matsui, H.; Grant, E. R. *J. Chem. Phys*. **1996**, *104*, 42. Mayer, E. E.; Hedderich, H.; Grant, E. R. *Philos. Trans. R. Soc. A* **1977**, *355*, 1569. Bell, P.; Aguirre, F.; Grant, E. R.; Pratt, S. T. *J. Chem. Phys*. **2003**, *119*, 10146. *J. Chem. Phys*. **2004**, *120*, 2667.

(5) Mayer, E. E.; Grant, E. R. *J. Chem. Phys*. **1995**, *103*, 10513. Mayer, E. E.; Hedderich, H. G.; Grant, E. R. *J. Chem. Phys*. **1998**, *108*, 1886. Mayer, E. E.; Hedderich, H. G.; Grant, E. R. *J. Chem. Phys*. **1998**, *108*, 8429. Robinson, J. D.; Foltynowicz, R. J.; Grant, E. R. *J. Chem. Phys*. **2000**, *112*, 1679−1684. Zückerman, E. J.; Mayer, E. E.; Foltynowicz, R. J.; Robinson, J. D.; Knopka, M.; Jen, S. H.; Chen, I.-C.; Hedderich, H. G.; Grant, E. R. *J. Chem. Phys*. **2000**, *113*, 5372.

(6) Tjossem, P. J. H.; Goodwin, P. M.; Cool, T. A. *J. Chem. Phys*. **1986**, *84*, 5334. Tjossem, P. J. H.; Cool, T. A.; Webb, D. A.; Grant, E. R. *J. Chem. Phys*. **1988**, *88*, 617.

(7) Song, X. M.; Cool, T. A. *J. Chem. Phys*. **1992**, *96*, 8664.

(8) Robinson, J. D.; Foltynowicz, R. J.; Prentice, K.; Bell, P.; Grant, E. R. *J. Chem. Phys*. **2002**, *116*, 8384.

(9) Hippler, M.; Pfab, J. *Chem. Phys. Lett*. **1995**, *243*, 500.

(10) Kolodney, E.; Powers, P. S.; Hodgson, L.; Reisler, H.; Wittig, C. *J. Chem. Phys*. **1991**, *94*, 2330.

(11) Uberna, R.; Hinchliffe, R. D.; Cline, J. I. *J. Chem. Phys*. **1996**, *105*, 9847.

(12) Ashworth, S. H.; Brown, J. M. *An Atlas of Optogalvanic Transitions in Neon*; Rutherford Appleton Laboratory: Oxford, 1991.

(13) Amano, T. *J. Chem. Phys*. **1983**, *79*, 3595.

(14) Gudeman, C. S.; Begemann, M. H.; Pfaff, J.; Saykally, R. J. *Phys. Rev. Lett*. **1983**, *50*, 727.

(15) Brown, J. M.; Radford, H. E.; Sears, T. J. *J. Mol. Spectrosc*. **1991**, *148*, 20.

(16) McKellar, A. R. W. *Discuss. Faraday Soc*. **1981**, *71*, 63.

(17) McKellar, A. R. W.; Burkholder, J. B.; Orlando, J. J.; Howard, C. J. *J. Mol. Spectrosc*. **1988**, *130*, 445.

(18) Landsberg, B. M.; Merer, A. J.; Oka, T. *J. Mol. Spectrosc*. **1977**, *67*, 459.

(19) Blake, G. A.; Sastry, K. V. L. N.; DeLucia, F. C. *J. Chem. Phys*. **1984**, *80*, 95.

(20) Watson, J. K. G. *Vibrational Spectra and Structure*; Amsterdam: Elsevier: 1977; Vol. 6.

(21) Brown, J. M.; Sears, T. J. *J. Mol. Spectrosc*. **1979**, *75*, 111.

(22) Gauyacq, D.; Jungen, Ch. *Mol. Phys*. **1980**, *41*, 383.

(23) Brown, J. M.; Jorgensen, F. *Mol. Phys*. **1982**, *47*, 1065.

(24) Hougen, J. T.; Jesson, J. P. *J. Chem. Phys*. **1963**, *38*, 1524.

(25) Brown, J. M. *J. Mol. Spectrosc*. **1977**, *68*, 412.

(26) Hougen, J. T. *J. Chem. Phys*. **1962**, *36*, 519.

(27) Zare, R. N. *Angular Momentum*; Wiley: New York, 1988.

(28) Kovacs, I. *Rotational Structure in the Spectra of Diatomic Molecules*; Elsevier: New York, 1969.

(29) Henderson, J. R.; Muramoto, M.; Willet, R. A. *J. Chem. Phys*. **1964**, *41*, 580.

(30) Mladenovic, M.; Schmatz, S. *J. Chem. Phys*. **1998**, *109*, 4456.

(31) Hirota, E. *J. Mol. Struct*. **1986**, *146*, 237.

(32) Murray, K. K.; Miller, T. M.; Leopold, D. G.; Lineberger, W. C. *J. Chem. Phys*. **1986**, *84*, 2520.

(33) Lorenzen-Schmidt, H.; Peric, M.; Peyerimhoff, S. D. *J. Chem. Phys*. **1993**, *98*, 525. Peric, M.; Peyerimhoff, S. D. *J. Chem. Phys*. **1993**, *98*, 3587.

(34) Kawaguchi, K.; Hirota, E.; Yamada, Y. *Mol. Phys*. **1981**, *44*, 509.

(35) Brown, J. M. *Mol. Phys*. **2003**, *101*, 3419.